AIP | Applied Physics Letters

In operandi observation of dynamic annealing: A case study of boron in germanium nanowire devices

Maria M. Koleśnik-Gray, Christian Sorger, Subhajit Biswas, Justin D. Holmes, Heiko B. Weber, and Vojislav Krstić

Citation: Applied Physics Letters **106**, 233109 (2015); doi: 10.1063/1.4922527
View online: http://dx.doi.org/10.1063/1.4922527
View Table of Contents: http://scitation.aip.org/content/aip/journal/apl/106/23?ver=pdfcov
Published by the AIP Publishing

In operandi observation of dynamic annealing: A case study of boron in germanium nanowire devices

Maria M. Koleśnik-Gray,[1,3,4] Christian Sorger,[1] Subhajit Biswas,[2,3] Justin D. Holmes,[2,3] Heiko B. Weber,[1] and Vojislav Krstić[1,3,4,a)]

[1]*Department of Physics, Chair for Applied Physics, Friedrich-Alexander University Erlangen-Nürnberg (FAU), Staudtstr. 7, 91058 Erlangen, Germany*
[2]*Materials Chemistry and Analysis Group, Department of Chemistry, Tyndall Institute, University College Cork, Cork, Ireland*
[3]*Centre for Research on Adaptive Nanostructures and Nanodevices (CRANN), and AMBER at CRANN, Trinity College Dublin, College Green, Dublin 2, Ireland*
[4]*School of Physics, Trinity College Dublin, College Green, Dublin 2, Ireland*

(Received 10 March 2015; accepted 3 June 2015; published online 11 June 2015)

We report on the implantation of boron in individual, electrically contacted germanium nanowires with varying diameter and present a technique that monitors the electrical properties of a single device during implantation of ions. This method gives improved access to study the dynamic annealing ability of the nanowire at room temperature promoted by its quasi-one-dimensional confinement. Based on electrical data, we find that the dopant activation efficiency is nontrivially diameter dependent. As the diameter decreases, a transition from a pronounced dynamic-annealing to a radiation-damage dominated regime is observed. © *2015 AIP Publishing LLC*.
[http://dx.doi.org/10.1063/1.4922527]

Germanium nanowires (Ge NWs) represent a nanoscaled semiconductor with the potential to replace and/or complement nanostructured silicon in future electronics while sustaining the progress of Moore's law.[1] Structurally stable Ge NWs can be synthetically produced with high yield and good control over the diameter size.[2,3] In order to achieve successful integration of Ge NWs into functional devices, means of controlled doping have to be established and evaluated. Although doping of NWs with shallow impurities such as boron and phosphorus can be realized during their synthesis,[4,5] this approach can be flawed due to the lack of control over the effective impurity levels, impurity segregation towards the surface, and the incorporation of other, undesired species into the NW body from the precursor material.[5]

Ion-beam implantation instead of *in-situ* synthesis doping is a technique routinely used for modification of electrical, optical, and magnetic properties in semiconductor technology and offers wider opportunities for NW doping.[6,7] Nevertheless, implantation doping of a semiconductor material is rather complex involving two competing processes, namely, the formation of undesired damage in the irradiated host crystal and the self-activation of the selected dopants. Self-activation originates from so-called dynamic annealing,[8] which involves migration of implanted ions onto substitutional lattice sites. However, at high doses, ion implantation results in significant amorphization of the semiconductor material, where the crystalline structure may be partially restored via thermal annealing. Radiative damage effects have been well studied in bulk semiconductors;[9] however, it has been suggested in view of the ion implantation theory that in NWs, the probability of dynamic annealing is promoted due to the specific quasi-one-dimensional (1D) confinement, resulting in slower dissipation of the ion impact-energy.[10,11]

In this manuscript, we present experiments in which implantation is carried out on an electrically side-contacted individual nanowire.[12] This has many advantages: (i) the dynamic annealing can be tracked *in operandi* by the electrical measurement upon ion implantation; (ii) the side contact geometry allows for doping only the conduction channel, while the buried contact is essentially unchanged; (iii) by the use of an ion implanter, any element can, in principle, be incorporated, in particular, the technologically relevant element B, and further allowing for scalable doping of integrated circuits with controlled dopant distributions and depth.

This technique complements the extensive studies in the past years that targeted changes in microscopic structure after ion implantation of semiconductor NWs with full area[13,14] and focused ion beam (FIB)[15,16] techniques. These elucidated ion-beam caused changes in morphology, with a resulting high defect density.[14,16] However, only a few studies can be found in literature concerning the modification of the electrical properties of synthetic NWs upon ion implantation.[17–19] In a recent work by Zeiner *et al.*,[17] a marked decrease in resistivity upon doping of device-integrated Ge NWs with Ga from a FIB source was demonstrated without thermal annealing. Other works on Si:Ga[18] (FIB) and Ge:B and Ge:P[19] (full area) NWs opted for adding the electrical contacts subsequent to the implantation. For the Si NWs electrical activation required a post-annealing step, that is, no dynamic annealing was observed.

Surprisingly, the correlation between the NW diameter and dynamic annealing efficiency has not been studied to date, despite the fact that the quasi-1D character of semiconductor NWs is mandatory for dynamic annealing and has huge impact on their electrical properties.[20] This can straightforwardly be studied with our *in operandi* technique.

a)E-mail: vojislav.krstic@fau.de

In our study, B ions were selected due to their reported low diffusivity and high degree of electrical activation in bulk Ge.[21] The effects of irradiation with B on charge transport are investigated by monitoring the change in NW and contact resistivity with incrementally increasing fluencies in the range of 10^{10}–$10^{15}\,cm^{-2}$ for NWs with diameter sizes of 29, 38, and 53 nm. The modification of microscopic structure of Ge NWs implanted with a dose of $5 \times 10^{15}\,cm^{-2}$ is studied via SEM and TEM.

Ge NWs with diameter sizes ranging from a few ten to 100 nm (Fig. 1(a)) were synthesized via a vapour-liquid-solid approach as described in Ref. 22. Our earlier studies[12,22,23] indicated that the as-grown NWs were *p*-type doped with carrier concentrations ranging from $3 \times 10^{17}\,cm^{-3}$ up to $10^{19}\,cm^{-3}$. This behaviour is characteristic for all non-intentionally doped synthetically derived Ge NWs.[24,25] Effective implantation of B at high fluencies was therefore expected to overcome the pre-existent doping and decrease the resistivity of the NWs for concentrations of activated dopants higher than the initial carrier concentrations.

For sample preparation, the NW material was diluted in isopropanol and dispersed on SiO_2 substrates. Individual NWs were contacted with 60 nm high Ag electrodes in four-terminal device configuration (Figs. 1(b) and 1(c)) using combined optical and electron-beam lithography. Additionally, open circuit two electrode structures (Fig. 1(b)) were produced to verify whether irradiation of the sample may cause formation of a thin conducting layer at or within the SiO_2 substrate.

Ion implantation was carried out using a 350 kV Heavy Ion Accelerator (HV Eng. Europa BV) at the pressure of 10^{-6} mbar. An energy of 20 keV was selected in order to achieve a broad implantation peak at a mean depth of 47 nm estimated by TRIM simulations,[26,27] which was deemed most suitable for Ge NWs within the available diameter range. Since the TRIM data were calculated for bulk Ge, the expected implantation profile and depth were taken as a rough reference point for the experiment.

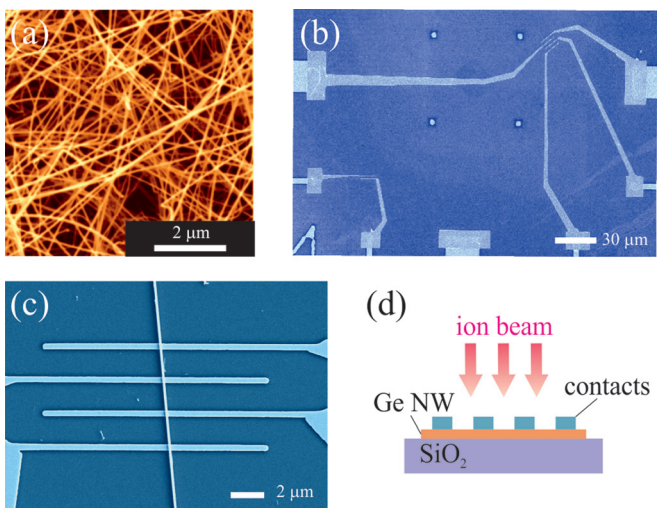

FIG. 1. SEM images of Ge NWs and associated nanodevices. (a) Bundles of Au-seeded Ge NWs deposited on SiO_2 surface, showing a wide diameter distribution (20–100 nm) of NWs with high aspect ratios. (b) SEM image of a four-terminal Ge NW device (top right) and an open-circuit two-terminal structure (bottom left). (c) Higher magnification SEM image of a four-terminal Ge NW device fabricated with 200 nm wide Au electrodes with 1 μm spacings. (d) Schematic diagram of the implantation procedure.

The NW longitudinal axis was aligned perpendicular to the ion beam (Fig. 1(d)). The B ions were implanted with incrementally increasing doses from 10^{11} up to $10^{15}\,cm^{-2}$. After each implantation step, current-voltage characteristics of the nanodevices ($I_d - V_{sd}$) and the NW channels ($I_d - V_{4T}$, four-terminal probing) were measured using an Agilent E5270B source-measure unit. Subsequently, the NW resistivity and contact-resistivity values were extracted from the measurement at different B fluencies based on the geometry of the devices.[12,27] We note that true live monitoring of the electrical properties during implantation is not the very best choice, as the ion impact on the metallic electrodes dominated the electrical signals, obscuring the dynamical annealing. Therefore, we have opted for a repeated sequential protocol, in which a short implantation time interval (few milliseconds) is immediately followed by a measurement interval.

To test the potential short-circuiting of the SiO_2 dielectric, open circuit structures were probed before and after sample irradiation using the same V_{sd} range as for the Ge NW devices.[27] The data show that there are no electrically conducting paths created within the oxide layer, and therefore, the implantation conditions do not compromise the electrical measurements on the individual NWs.

Fig. 2 shows representative data for B implantation of a 53 nm diameter Ge NW. The NW resistivity, ρ_{NW}, (Fig. 2(a)), and contact-resistivity, ρ_C (Fig. 2(b)) are plotted as function of boron implant fluency. Based on the results of electrical characterization, three main stages (I–III) of implantation doping can be identified,[28] depending on which of the two competing processes — damage production or dopant activation — dominates in a given stage, as denoted in Fig. 2(a).

In the low-fluency range (10^{11}–$3 \times 10^{13}\,cm^{-2}$), denoted as stage I, fluctuations in ρ_{NW} and ρ_C within one order of magnitude are observed. In this dose range, defect formation counteracts the effective doping of the material; therefore, the fluctuations are associated with characteristic series of defect formation (increasing) and damage removal (decreasing resistivity) events.

At fluencies exceeding $3 \times 10^{13}\,cm^{-2}$ (stage II), a sharp drop in ρ_{NW} and ρ_C by two to three orders of magnitude is observed. This is characteristic of the dynamic annealing dominating over damage by ion irradiation of the NW material. The implant fluency at which the effective doping becomes dominant over defect formation can be defined as the *doping threshold dose*. The doping threshold dose mainly depends on the initial carrier concentrations of the implanted NWs. Therefore, the wide span of fluencies in stage I is a consequence of high synthesis-caused pre-existent doping of the NWs, as the equivalent concentration of activated B acceptor levels is needed to exceed the initial acceptor density. With further increasing fluencies, the device signal was eventually lost (stage III). Subsequent SEM imaging revealed that the devices underwent significant electromigration damage in both the channels and the contact-interfaces.[27] The onset of electromigration is assigned to extensive amorphization-related damage in the NWs at high boron

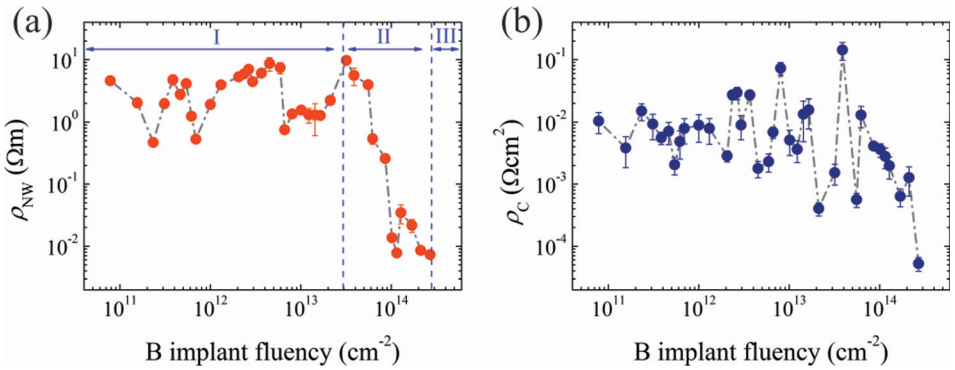

FIG. 2. Electrical characterization of ion implantation doping in Ge NWs. Representative data for a 53 nm diameter NW show (a) the NW resistivity ρ_{NW} and (b) contact resistivity ρ_C plotted as function of the nominal implanted dose. Three stages of characteristic defect formation and activation can be distinguished, denoted in (a). At fluencies below $3 \times 10^{13}\,\mathrm{cm}^{-2}$ (stage I), ρ_{NW} and ρ_C values fluctuate slowly within one order of magnitude since the density of activated B dopants in this fluency range is smaller than the initial carrier concentration in the NWs. For higher doses (stage II), beyond a threshold doping dose, a distinct drop in ρ_{NW} and ρ_C signifies the effective B doping of the NW. Finally, above $3 \times 10^{14}\,\mathrm{cm}^{-2}$ (stage III), the device signal was lost due to Joule-heating mediated electromigration resulting from an onset of amorphization of the NW.

fluencies. Presumably, the dynamic annealing becomes inefficient at too high levels of strain-disorder. Therefore, the fluency at which device signal was lost can be defined as the *amorphization dose*.

The doping threshold and amorphisation doses were found to exhibit a diameter dependence, as shown in Fig. 3(a). Larger diameter NWs are more resilient to amorphization damage. Also, the doping threshold dose increases with diameter size.

The extent of NW and contact-resistivity change as function of diameter size is illustrated in Figs. 3(b) and 3(c). The ratio for ρ_{NW} and ρ_C at stages III and I (denoted by corresponding superscripts) is plotted as function of NW diameter. Clearly, the tendency for reduction of NW and contact-resistivity after implantation becomes stronger with increasing NW diameter size. Remarkably, for a 29 nm NW, a weak increase in ρ_{NW} is observed, indicating the dominance of radiation-related damage over dynamic annealing in the full dose range.

To elaborate further the diameter-dependent effect observed during the electrical characterization, Ge NWs were drop-cast on TEM grids and implanted with B to the fluency of $5 \times 10^{14}\,\mathrm{cm}^{-2}$, that is, beyond the amorphization dose as found in the electrical results. Fig. 4 shows SEM and

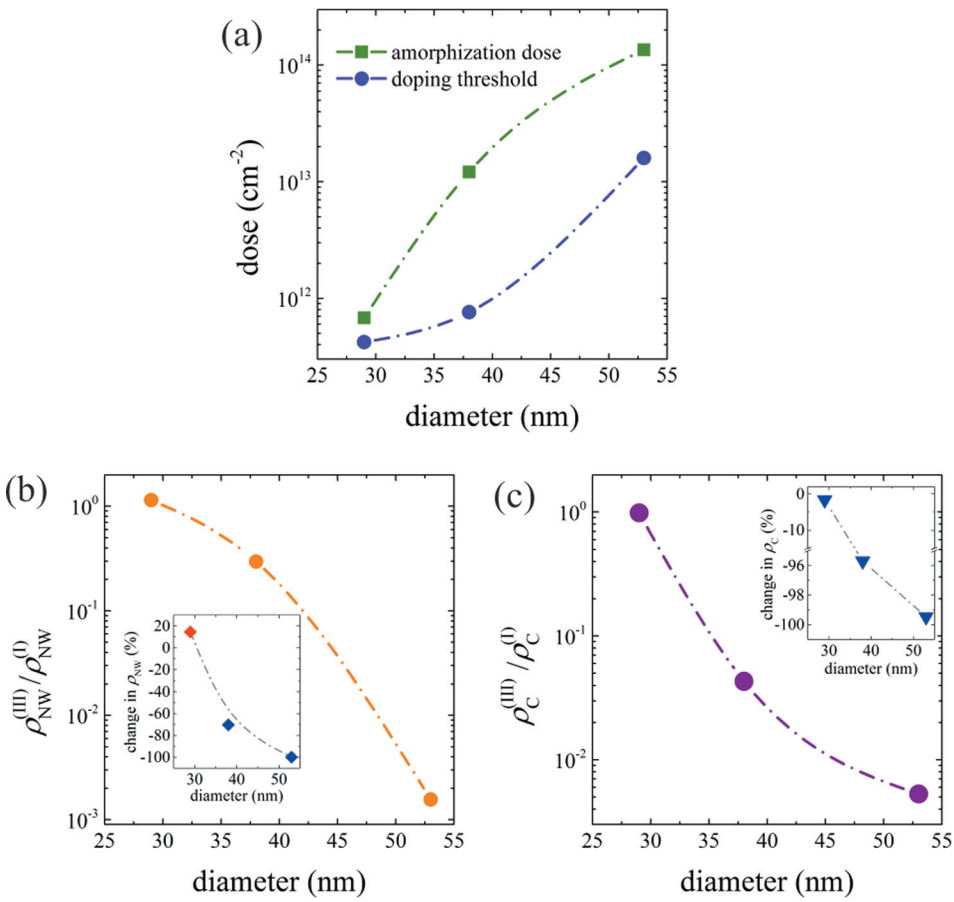

FIG. 3. Diameter-dependence of ion implantation doping effects in Ge NWs. (a) Doping threshold and amorphization dose plotted as function of diameter size. Larger diameter NWs are more resilient to implantation damage. Dashed-dotted lines are guides to the eye. (b) Relative change, $\rho^{(III)}/\rho^{(I)}$, in NW resistivity and (c) contact-resistivity as function of NW diameter, comparing resistivities in stages III and I of the implantation process. Insets in (b) and (c) show the overall change (in %) in the respective resistivities. The results indicate that as the NW diameter decreases, the probability of dopant activation becomes smaller while defect formation is more extensive. Dashed-dotted lines are guides to the eye.

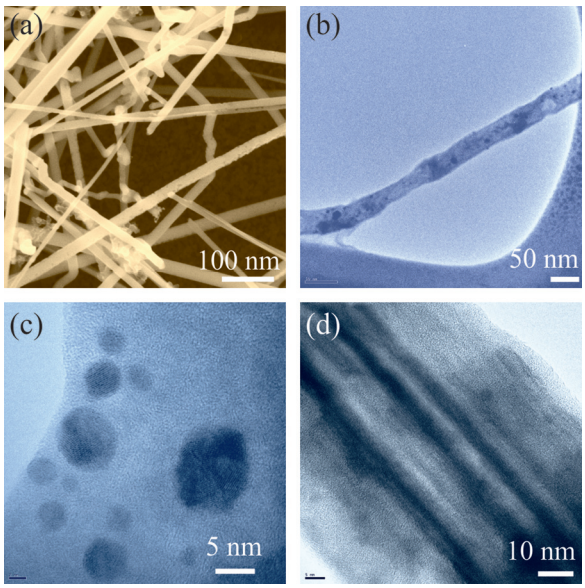

FIG. 4. Surface morphology and crystalline structure of Ge NWs implanted with B to the dose of $5 \times 10^{14}\,cm^{-2}$. (a) SEM image of B implanted Ge NWs deposited on SiO_2 surface. NWs with diameters below about 45 nm show increased surface roughness, whereas thicker NWs remain a smooth surface. (b) TEM image of a 36 nm wire, showing a large number of defects spread all over the NW body. (c) TEM image of crystalline clusters embedded beneath amorphized Ge NW surface (55 nm). (d) High number of stacking faults associated with the incorporation of B clusters in a 82 nm longitudinally twinned Ge NW.

TEM images of NWs after implantation. SEM imaging (Fig. 4(a)) revealed slight surface roughening and blistering for NWs with diameters below 40 nm, whereas for larger diameter NWs, there is no or very little appreciable tendency for such change in the surface morphology. TEM imaging revealed a more detailed structure of radiation-related damage in the NW body, with clusters of B distributed all over the NW thickness (Fig. 4(b)) and embedded within an amorphized Ge matrix. Interestingly, the B clusters do not seem to have segregated towards the NW surface (Figs. 4(c) and 4(d)), which however was reported to be the case for NWs doped during synthesis.[5] This indicates a different hetero-atom dynamics in Ge NWs depending on whether hetero-atoms are introduced by post-implantation or *in-situ* during synthesis. Furthermore, as was expected from the electrical data, irradiation of thinner NWs caused the most damage to the material, with significant amorphization, blistering, and breakages of the NWs. In thicker NWs, the implantation-related damage was less pronounced (Fig. 4(d)) with a large number of dislocation centres formed within the weakly amorphized crystalline structure.[27]

Summarizing, the presented results provide insight into the diameter-dependence of ion-implantation effectiveness for device-integrated sub-100 nm diameter Ge NWs. Electrical activation of B dopants at room temperature is demonstrated by a marked decrease in NW and contact-resistivity at high fluencies, likely promoted by the quasi-1D confinement of the NWs. The observed diameter dependence demonstrates that the resistivity reduction due to doping decreases with shrinking NW diameter. In particular, once the NW diameter falls below few tens of nm, the NW's ability of dynamic annealing is reduced and the amorphization probability of the NWs due to the impacting ions becomes stronger. These findings have been enabled by application of a powerful technique that is *in operandi* tracking of the electrical properties during implantation. This very general methodology, suited for any dopant, paves the way for a detailed understanding of dynamic annealing in device-integrated semiconductor NWs and associated electronic properties.

This work was funded by the Science Foundation Ireland (PI Award 08/IN.1/I1873 and CSET 08/CE/I1432). V.K. and H.B.W. supervised the project and the associated studies. M.M.K prepared the devices. M.M.K and C.S. carried out the measurements. S.B. and J.D.H. provided the semiconductor nanowires. All authors contributed to the manuscript write-up.

[1]B. Yu, X. H. Sun, G. A. Calebotta, G. R. Dholakia, and M. Meyyappan, J. Clust. Sci. **17**, 579 (2006).
[2]G. Gu, M. Burghard, G. T. Kim, G. S. Düsberg, P. W. Chiu, V. Krstić, S. Roth, and W. Q. Han, J. Appl. Phys. **90**, 5747 (2001).
[3]C. O'Regan, S. Biswas, N. Petkov, and J. D. Holmes, J. Mater. Chem. C **2**, 14 (2014).
[4]E. Tutuc, S. Guha, and J. O. Chu, Appl. Phys. Lett. **88**, 043113 (2006).
[5]D. E. Perea, E. R. Hemesath, E. J. Schwalbach, J. L. Lensch-Falk, P. W. Voorhees, and L. J. Lauhon, Nat. Nanotechnol. **4**, 315 (2009).
[6]J. S. Williams, Mater. Sci. Eng. A **253**, 8 (1998).
[7]C. Fritzsche, Angew. Chem. **17**, 496 (1978).
[8]E. Chason, S. T. Picraux, J. M. Poate, J. O. Borland, M. I. Current, T. Diaz de la Rubia, D. J. Eaglesham, O. W. Holland, M. E. Law, C. W. Magee, J. W. Mayer, J. Melngailis, and A. F. Tasch, J. Appl. Phys. **81**, 6513 (1997).
[9]K. S. Jones, S. Prussin, and E. R. Weber, Appl. Phys. A **45**, 1 (1988).
[10]S. Dhara, A. Datta, C. T. Wu, Z. H. Lan, K. H. Chen, Y. L. Wang, L. C. Chen, C. W. Hsu, H. M. Lin, and C. C. Chen, Appl. Phys. Lett. **82**, 451 (2003).
[11]G. Ouyang, G. Yang, and G. Zhou, Nanoscale **4**, 2748 (2012).
[12]M. M. Koleśnik-Gray, T. Lutz, G. Collins, S. Biswas, J. D. Holmes, and V. Krstić, Appl. Phys. Lett. **103**, 153101 (2013).
[13]C. Ronning, C. Borschel, S. Geburt, and R. Niepelt, Mater. Sci. Eng. **70**, 30 (2010).
[14]D. Stichtenoth, K. Wegener, C. Gutsche, I. Regolin, F. J. Tegude, W. Prost, M. Seibt, and C. Ronning, Appl. Phys. Lett. **92**, 163107 (2008).
[15]N. Petkov, R. Kelly, M. Schmidt, and J. D. Holmes, in *Proceedings of the 15th European Microscopy Congress, Manchester, United Kingdom, 16–21 September 2012* (Royal Microscopical Society, 2012).
[16]N. Petkov, ISRN Nanotechnol. **2013**, 893060 (2013).
[17]C. Zeiner, A. Lugstein, T. Burchhart, P. Pongratz, J. G. Connell, L. J. Lauhon, and E. Bertagnolli, Nano Lett. **11**, 3108 (2011).
[18]A. Colli, A. Fasoli, C. Ronning, S. Pisana, S. Piscanec, and A. C. Ferrari, Nano Lett. **8**, 2188 (2008).
[19]T. Burchhardt, C. Zeiner, A. Lugstein, C. Henkel, and E. Bertagnolli, Nanotechnology **22**, 035201 (2011).
[20]F. G. Pikus and K. K. Likharev, Appl. Phys. Lett. **71**, 3661 (1997).
[21]V. P. Kesan, S. S. Iyer, and J. M. Cotte, Appl. Phys. Lett. **59**, 852 (1991).
[22]G. Collins, M. M. Koleśnik, V. Krstić, and J. D. Holmes, Chem. Mater. **22**, 5235 (2010).
[23]S. Barth, M. M. Koleśnik, K. Donegan, V. Krstić, and J. D. Holmes, Chem. Mater. **23**, 3335 (2011).
[24]A. B. Greytak, L. J. Lauhon, M. S. Gudiksen, and C. M. Lieber, Appl. Phys. Lett. **84**, 4176 (2004).
[25]S. Zhang, E. R. Hemesath, D. E. Perea, E. Wijaya., J. L. Lensch-Falk, and L. J. Lauhon, Nano Lett. **9**, 3268 (2009).
[26]J. F. Ziegler, *The Stopping and Range of Ions in Solids* (Pergamon, 1985).
[27]See supplementary material at http://dx.doi.org/10.1063/1.4922527 for information on electrical measurement details, ion implantation, trim data, EDX analysis, and TEM images of implanted nanowires.
[28]K. Lorenz, E. Alves, E. Wendler, O. Bilani, W. Wesch, and M. Hayes, Appl. Phys. Lett. **87**, 191904 (2005).